micromachines

MDPI

Article

Phase Formation Behavior and Thermoelectric Transport Properties of S-Doped $FeSe_{2-x}S_x$ Polycrystalline Alloys

Okmin Park †, Se Woong Lee †, Sang Jeong Park and Sang-il Kim *

Department of Materials Science and Engineering, University of Seoul, Seoul 02504, Republic of Korea
* Correspondence: sang1.kim@uos.ac.kr
† These authors contributed equally to this work.

Abstract: Some transition-metal dichalcogenides have been actively studied recently owing to their potential for use as thermoelectric materials due to their superior electronic transport properties. Iron-based chalcogenides, $FeTe_2$, $FeSe_2$ and FeS_2, are narrow bandgap (~1 eV) semiconductors that could be considered as cost-effective thermoelectric materials. Herein, the thermoelectric and electrical transport properties $FeSe_2$–FeS_2 system are investigated. A series of polycrystalline samples of the nominal composition of $FeSe_{2-x}S_x$ (x = 0, 0.2, 0.4, 0.6, and 0.8) samples are synthesized by a conventional solid-state reaction. A single orthorhombic phase of $FeSe_2$ is successfully synthesized for x = 0, 0.2, and 0.4, while secondary phases (Fe_7S_8 or FeS_2) are identified as well for x = 0.6 and 0.8. The lattice parameters gradually decrease gradually with S content increase to x = 0.6, suggesting that S atoms are successfully substituted at the Se sites in the $FeSe_2$ orthorhombic crystal structure. The electrical conductivity increases gradually with the S content, whereas the positive Seebeck coefficient decreases gradually with the S content at 300 K. The maximum power factor of 0.55 mW/mK^2 at 600 K was seen for x = 0.2, which is a 10% increase compared to the pristine $FeSe_2$ sample. Interestingly, the total thermal conductivity at 300 K of 7.96 W/mK (x = 0) decreases gradually and significantly to 2.58 W/mK for x = 0.6 owing to the point-defect phonon scattering by the partial substitution of S atoms at the Se site. As a result, a maximum thermoelectric figure of merit of 0.079 is obtained for the $FeSe_{1.8}S_{0.2}$ (x = 0.2) sample at 600 K, which is 18% higher than that of the pristine $FeSe_2$ sample.

Keywords: $FeSe_2$; FeS_2; thermoelectric; chalcogenides

check for updates

Citation: Park, O.; Lee, S.W.; Park, S.J.; Kim, S.-i. Phase Formation Behavior and Thermoelectric Transport Properties of S-Doped $FeSe_{2-x}S_x$ Polycrystalline Alloys. *Micromachines* **2022**, *13*, 2066. https://doi.org/10.3390/mi13122066

Academic Editor: Subhajit Roychowdhury

Received: 14 October 2022
Accepted: 22 November 2022
Published: 25 November 2022

Publisher's Note: MDPI stays neutral with regard to jurisdictional claims in published maps and institutional affiliations.

Copyright: © 2022 by the authors. Licensee MDPI, Basel, Switzerland. This article is an open access article distributed under the terms and conditions of the Creative Commons Attribution (CC BY) license (https://creativecommons.org/licenses/by/4.0/).

1. Introduction

Thermoelectric materials have been widely studied in recent years, owing to their ability to convert waste thermal gradients into electrical energy [1]. The energy-conversion efficiency of thermoelectric materials can be evaluated using the dimensionless thermoelectric figure of merit, zT, which is expressed by the following Equation (1).

$$zT = \frac{\sigma S^2}{\kappa_{tot}} T \quad (1)$$

where σ, S, T, and κ_{tot} are the electrical conductivity, Seebeck coefficient, absolute temperature, and total thermal conductivity, respectively [2–4]. Generally, κ_{tot} is divided into two terms:

$$\kappa_{tot} = \kappa_{elec} + \kappa_{latt} \quad (2)$$

where κ_{elec} and κ_{latt} are the electrical and lattice thermal conductivities, respectively. zT can be improved by increasing the power factor ($\sigma \cdot S^2$) or reducing κ_{tot}. However, the trade-off between σ and S and the proportionate relationship between σ and κ_{elec} make it difficult to improve zT. One strategy to obtain a high zT is to reduce κ_{latt} via point-defect phonon scattering, which can be achieved by doping or using a partial solid solution [5,6]. For example, Asfandiyar et al. investigated the thermoelectric properties of alloyed samples

in an SnS–SnSe system, and they reported that the κ_{latt} of the alloyed samples was lower than that of the nonalloyed samples, and that the zT of the alloyed samples was greatly enhanced [7].

Transition-metal dichalcogenides (TMDCs) such as $HfSe_2$ [8,9], $HfTe_2$ [10], $MoSe_2$ [11], and $SnSe_2$ [12,13] have attracted significant attention because of their high potential for use as thermoelectric materials. Generally, TMDCs have a large effective mass owing to the presence of local *d*- or *f*-orbital electrons, leading to a large magnitude of S [14]. Among these TMDCs, $FeSe_2$ and FeS_2 have been actively investigated as promising thermoelectric materials. $FeSe_2$ is a *p*-type semiconductor with a narrow direct bandgap of ~1 eV [15]. $FeSe_2$ is known to be thermally and structurally stable, as previous studies have reported [16,17]. It has a high carrier concentration, of 10^{18}–10^{19} cm^{-3}, and is considered a good candidate for thermoelectric applications [17,18]. FeS_2 is a semiconductor with a narrow bandgap (~1 eV) and is one of the most abundant sulfides in the Earth's crust [19]. It is nontoxic, inexpensive, and is considered a promising cost-effective thermoelectric material. By combining the first-principles calculations with the Boltzmann transport theory, Harran et al. predicted that the zT of FeS_2 could reach approximately 0.45 [20,21].

In this study, the electrical and thermoelectric transport properties of a series of polycrystalline $FeSe_{2-x}S_x$ (x = 0, 0.2, 0.4, 0.6, and 0.8) samples of the $FeSe_2$–FeS_2 system are investigated. The S substitution for the Se site was successful up to S content of x = 0.6. The σ increased gradually with the S content, whereas the positive S decreased gradually with the S content at 300 K. The weighted mobility of the samples is calculated and analyzed to understand the electrical transport properties better. With an increase in S content, the κ_{latt} decreases gradually and significantly.

2. Experimental Section

Polycrystalline $FeSe_{2-x}S_x$ (x = 0, 0.2, 0.4, 0.6, and 0.8) samples were synthesized via a conventional solid-state reaction in vacuum-sealed quartz tubes. High-purity raw materials: Fe (99.9%, Kojundo Chemical Laboratory Co., Ltd., Tolya, Japan), Se (99.999%, 5 N Plus), and S (99.995%, Sigma-Aldrich, St. Louis, MO, USA) were weighed stoichiometrically and heated at 833 K for 48 h. The obtained ingots were pulverized into powder using a ball-milling machine (SPEX 8000D, SPEX, Costa Mesa, CA, USA). Each powder sample was densified through spark plasma sintering (SPS-1030, Sumitomo Coal Mining Co. Ltd., Japan) at 803 K for 7 min under a pressure of 75 MPa. The crystalline structures of the sintered samples were identified through X-ray diffraction (XRD, D8 Discover, Bruker, Billerica, MA, USA) using Cu $K_{\alpha 1}$ radiation. Energy-dispersive X-ray spectroscopy (EDS) and EDS mapping were measured by secondary electron microscopy (SEM). The thermoelectric transport properties (σ and S) of the samples were measured using a thermoelectric evaluation system (ZEM-3M8, Advance Riko, Kanagawa prefecture, Japan) in the temperature range of 300–600 K. Hall measurements were conducted in the van der Pauw configuration using a Hall measurement system (HMS-5300, Ecopia, Korea) at 300 K. The thickness of the specimen for Hall measurement were 0.75, 0.73, 0.70 and 0.70 mm for x = 0, 0.2, 0.4, and 0.6, respectively, and the applied electric current and magnitude of the magnetic field were 20 mA and 0.553 T, respectively. The κ_{tot} of each sample was calculated as follows:

$$\kappa_{tot} = \alpha \rho C_p \quad (3)$$

where α, ρ, and C_p are the thermal diffusivity, density, and specific heat capacity, respectively. The α of the samples were measured in the range of 300–600 K through laser flash analysis (LFA457, Netzsch, Germany). Theoretical densities (D_x) of $FeSe_2$ and FeS_2 are 7.125 and 4.882 g/cm^3 (JCPDS #01-079-1892 and JCPDS #00-037-0375) respectively, and the D_x for the alloyed samples were considered to be the average value according to the solid solution ratio; the D_x values for the samples were 7.13, 6.90, 6.68, 6.45, and 6.23 g/cm^3 for x = 0, 0.2, 0.4, 0.6, and 0.8, respectively. The bulk densities for the samples were measured using the Archimedes method, and the relative densities were obtained from D_x and bulk densities. The calculated relative density values were 99.7, 98.9, 98.3, 98.3, and 97.8% for x = 0, 0.2,

0.4, 0.6, and 0.8, respectively. The C_p for the samples was measured using a differential scanning calorimeter (DSC8000, Perkin Elmer, Waltham, MA, USA).

3. Results and Discussion

Figure 1a shows the XRD patterns of the sintered samples of $FeSe_{2-x}S_x$ (x = 0, 0.2, 0.4, 0.6, and 0.8). The samples with x = 0, 0.2, and 0.4 exhibited a single orthorhombic phase ($FeSe_2$, JCPDS #01-079-1892) without any impurity. However, for the samples with higher S content (x = 0.6 and 0.8), a secondary phase (Fe_7S_8, JCPDS #01-089-1954) was identified. For the sample with x = 0.8, the peak intensity of the Fe_7S_8 secondary phase was increased and a small amount of FeS_2 was observed. The relative peak intensities remain similar for the samples with x = 0, 0.2, 0.4, and 0.6 (See Table S1 in Supplementary Materials). In addition, the grain sizes D for the samples (x = 0, 0.2, 0.4, and 0.6) were estimated using the Scherrer equation [22]:

$$D = \frac{K\lambda}{\beta \cos\theta} \tag{4}$$

where K, λ, θ, and β are the Scherrer constant, the wavelength of the X-ray beam, Bragg angle, and full width at half maximum, respectively. The K value of 0.94 was used, assuming the spherical crystallites. The calculated D values for the samples were 39.8, 39.2, 32.2, and 24.8 nm for x = 0, 0.2, 0.4, and 0.6, respectively. Even though the grain size of x = 0.6 is a bit smaller (possibly due to secondary phase formation), it can be known that there is no large difference in microstructures between samples of x = 0, 0.2, 0.4, and 0.6. The lattice parameters a, b, and c for the $FeSe_{2-x}S_x$ (x = 0, 0.2, 0.4, 0.6, and 0.8) crystal structures were calculated and are shown with error bars in Figure 1b. All lattice parameters decreased gradually with an increase in S content when $x < 0.8$, which confirmed that S atoms were successfully substituted at Se sites in the $FeSe_2$ crystal structure (the ionic radii of S^{2-} and Se^{2-} are 170 and 184 pm, respectively). However, the lattice parameters a, b, and c for x = 0.8, exhibited values similar to that for x = 0.6, suggesting that further S substitution at Se sites was limited. The EDS-SEM results are shown in Figure S1 and the atomic ratios measured by EDS-SEM are shown in Table S2 (Supplementary Information). The S-excess/Se-deficient regions are seen for x = 0.8, where the secondary phases started to be seen. The overall compositional ratios of S increases as S doping increases (Table S2 in Supplementary Information).

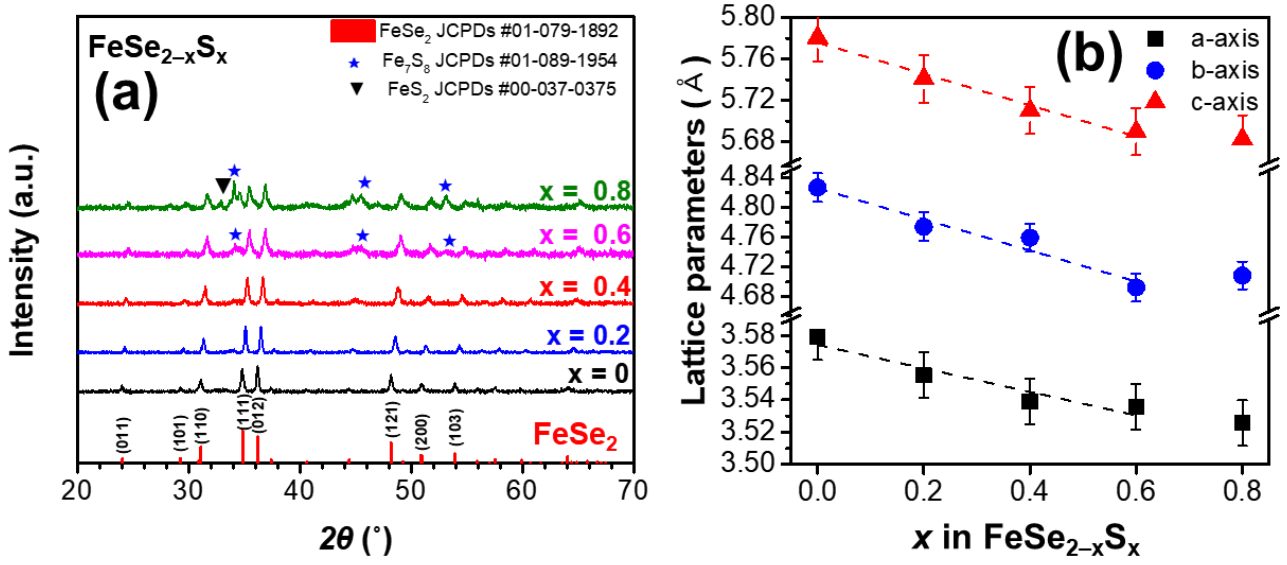


Figure 1. (**a**) XRD patterns of the series of $FeSe_{2-x}S_x$ (x = 0, 0.2, 0.4, 0.6, 0.8, and 1) samples. (**b**) Lattice parameters calculated using the XRD patterns.

Figure 2a shows the σ values of the $FeSe_{2-x}S_x$ (x = 0, 0.2, 0.4, and 0.6) samples. The sample with x = 0.8 with extensive secondary phases, which did not show the gradual decrease in lattice parameters, exhibited much higher σ values ~440 S/cm at 300 K (Not shown in Figure 2a). The thermoelectric measurement data of the x = 0.8 sample is not included due to the non-systematic change due to the existence of the secondary phases. The σ of the samples increased with temperature, exhibiting intrinsic semiconducting behavior. The σ values were 12.4, 15.3, 19.8, and 49.6 S/cm at 300 K, and 247, 315, 353, 442, and 1170 S/cm at 600 K for x = 0, 0.2, 0.4, and 0.6, respectively. The value of σ increased gradually with an increase in S content, over the entire temperature range. The relationship between σ and T can be expressed by the Arrhenius relationship [23]:

$$\sigma = \sigma_0 \exp(-E_a/kT) \quad (5)$$

where k is the Boltzmann constant and E_a is the activation energy. The inset in Figure 2b shows the Arrhenius relationship (logarithmic σ as a function of $1000/T$) for the samples and Figure 2b shows the calculated E_a with respect to x. Noticeable changes in the slope were observed at 400–450 K (Inset of Figure 2b). The calculated E_a values of the samples were 0.033, 0.032, 0.028, 0.013, and 0.006 eV in the low-temperature range and 0.123, 0.115, 0.114, 0.108, and 0.048 eV in the high-temperature range for x = 0, 0.2, 0.4, 0.6, and 0.8, respectively. The E_a decreased gradually with an increase in S content in both low- and high-temperature ranges.

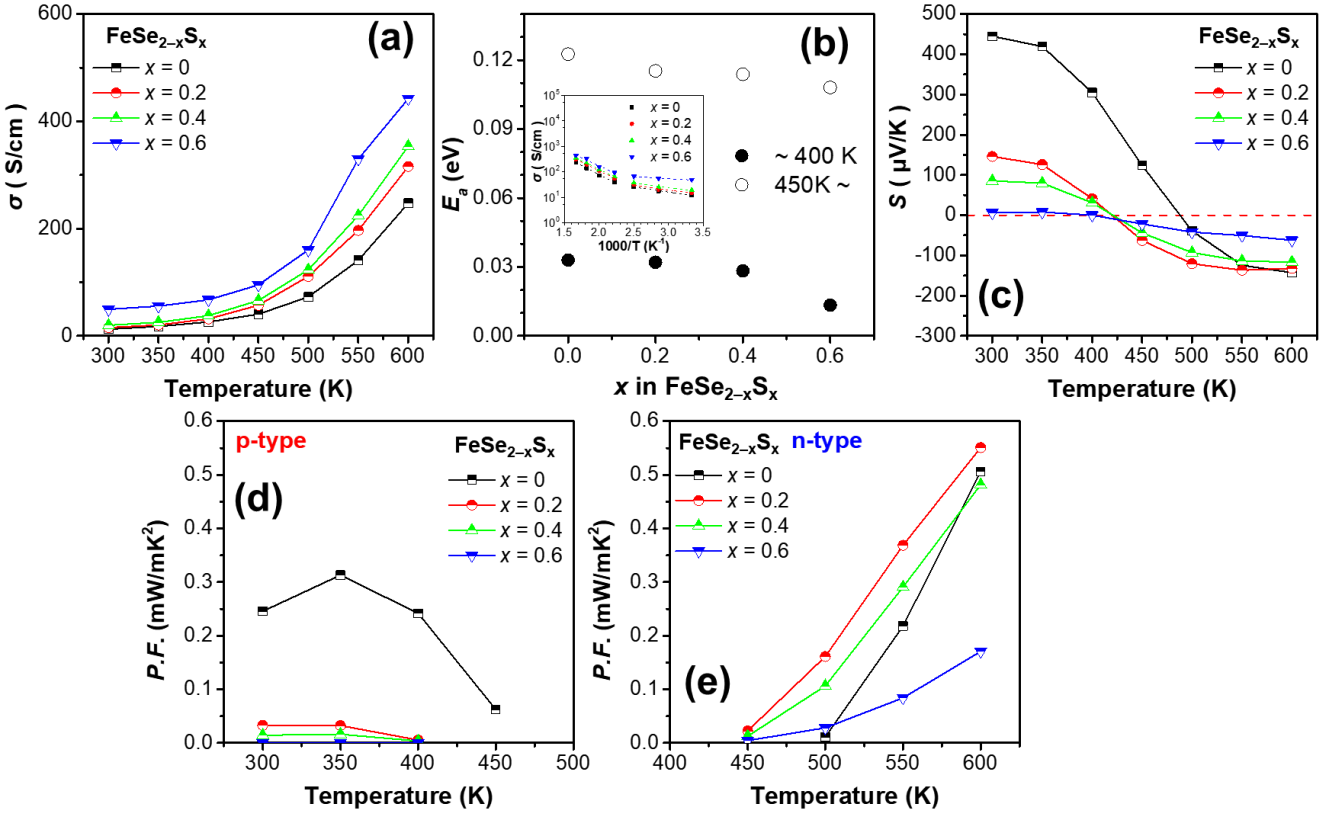


Figure 2. (**a**) σ as a function of the temperature for the series of $FeSe_{2-x}S_x$ (x = 0, 0.2, 0.4, 0.6, and 0.8) samples. (**b**) E_a of the samples calculated from σ for 300–400 K and 450–600 K. The inset of (**b**) shows logarithmic σ as a function of $1000/T$ for the samples. (**c**) S as a function of temperature for the samples. Power factors as functions of temperature for the samples in (**d**) p- and (**e**) n-type regions.

Figure 2c shows S as a function of the temperature for the $FeSe_{2-x}S_x$ (x = 0, 0.2, 0.4, and 0.6) samples. The S values of the samples at 300 K were 445, 146, 85, and 6 μV/K for x = 0, 0.2, 0.4, and 0.6, respectively. All the samples exhibited positive S values at 300 K,

showing *p*-type conduction: however, the conduction changes to *n*-type at 400–500 K. At higher temperatures, the *S* values of all the samples became negative and the *S* values of the samples at 600 K were gradually decreases from −143 to −62 μV/K. Interestingly, the magnitude of *S* decreased gradually with increasing S content at both 300 and 600 K.

Figure 2d,e shows the calculated power factors of the samples where the conduction is *p*- and *n*-type, respectively, according to the temperature range. In Figure 2d, the power factor of *p*-type conduction was the highest for the pristine $FeSe_2$ sample ($x = 0$), exhibiting a maximum value of 0.31 mW/mK^2 at 350 K. The power factors of the alloyed samples ($x = 0$, 0.2, 0.4, and 0.6) were lower than that of the pristine sample, despite the increase in σ, mainly owing to the significant decrease in *S* at the low-temperature range. However, when considering the power factor of the *n*-type conduction, the power factor at 600 K of $x = 0.2$ and 0.4 was comparable to the pristine sample (the power factors of the samples at 600 K were 0.50, 0.55, 0.48, 0.17, and 0.051 mW/mK^2 for $x = 0$, 0.2, 0.4, 0.6, and 0.8, respectively). The power factor of the sample with $x = 0.2$ was the highest, which could be attributed to an increase in σ and a small decrease in the magnitude of *S*. Therefore, a maximum power factor of 0.55 mW/mK^2 was achieved for the sample with $x = 0.2$ at 600 K, which was 10% higher than that of pristine $FeSe_2$. The sample of $x = 0.6$ exhibits lower power factors due to a large decrease in the magnitude of *S*.

Figure 3a,b present the Hall carrier concentration (n_H) and Hall mobility (μ_H) of the samples, measured at 300 K. The n_H values were 1.67×10^{19}, 1.81×10^{19}, 1.91×10^{19}, and 3.80×10^{19} cm^{-3} and the μ_H values were 4.01, 4.90, 5.97, and 6.44 cm^2/Vs, for $x = 0$, 0.2, 0.4, and 0.6, respectively. All the samples exhibited positive n_H values at 300 K, and n_H and μ_H increased gradually with an increase in *x*. Thus, the increase in the σ of the samples could be due to the simultaneous increase in n_H and μ_H. Furthermore, an increase in carrier concentration generally leads to a decrease in the magnitude of *S*, according to the Mott relationship [24]:

$$S = \frac{8\pi^2 k^2}{3eh^2} m_d^* T \left(\frac{\pi}{3n}\right)^{\frac{2}{3}}, \quad (6)$$

where m_d^*, *e*, and *h* are the density-of-state effective mass, elementary charge, and Planck's constant, respectively. Therefore, the decrease in the magnitude of *S* for the alloyed samples at 300 K could be attributed to the increase in n_H. Figure 3c,d show the m_d^* values of the samples at 300 K calculated using the measured *S* and n_H, based on the relationship in Equation (6). The m_d^* values of the samples were 1.45, 0.50, 0.30, and 0.04 m_0 for $x = 0$, 0.2, 0.4, and 0.6, respectively. The m_d^* values decreased gradually with an increase in S content.

Figure 3e shows the weighted mobility (μ_w) of the samples, obtained for a better understanding of the thermoelectric properties of the samples. The μ_w was calculated using the measured σ and *S* from a simple analytic form that approximates the exact Drude–Sommerfeld free-electron model for $|S| > 20$ μV/K [25]:

$$\mu_w = \frac{3h^3\sigma}{8\pi e(2m_e kT)^{3/2}} \left[\frac{\exp\left[\frac{|S|}{k/e} - 2\right]}{1 + \exp\left[-5\left(\frac{|S|}{k/e} - 1\right)\right]} + \frac{\frac{3}{\pi^2}\frac{|S|}{k/e}}{1 + \exp\left[5\left(\frac{|S|}{k/e} - 1\right)\right]} \right], \quad (7)$$

where m_e is the electron mass. μ_w is closely related to the theoretically optimum electrical performance of a thermoelectric material, and is relevant to the maximum power factor when n_H is tuned properly [26]. Therefore, the μ_w trend was very similar to that of the power factor. The values of μ_w at 600 K were 20.3, 22.7, 20.9, and 11.9 cm^2/Vs for $x = 0$, 0.2, 0.4, and 0.6, respectively. The μ_w increased initially at $x = 0.2$ and decreased gradually at $x > 0.2$, which was in agreement with the power factor trend at 600 K.

Figure 4a,b show the κ_{tot} and κ_{latt} of the samples as functions of temperature. The inset of Figure 4a shows the temperature dependence of κ_{elec}. The κ_{elec} of the samples was calculated according to the Wiedemann–Franz law [27]:

$$\kappa_{elec} = L\sigma T \quad (8)$$

where L is the Lorenz number. Subsequently, the κ_{latt} was calculated by subtracting κ_{elec} from κ_{tot}. The electronic contribution to κ_{tot} was not very significant; thus, κ_{tot} and κ_{latt} exhibited similar values. The κ_{latt} values of the samples were 7.96, 6.07, 4.47, and 2.58 W/mK at 300 K and 4.29, 3.85, 3.51, and 2.10 W/mK at 600 K, for x = 0, 0.2, 0.4, and 0.6, respectively. The κ_{latt} decreased gradually as the S content increased, over the entire temperature range, which was attributed to the point-defect phonon scattering caused by the partial substitution of S atoms at Se sites (the atomic masses of S and Se are 32.065 and 78.96 amu and the ionic radii of S^{2-} and Se^{2-} are 170 and 184 pm, respectively).

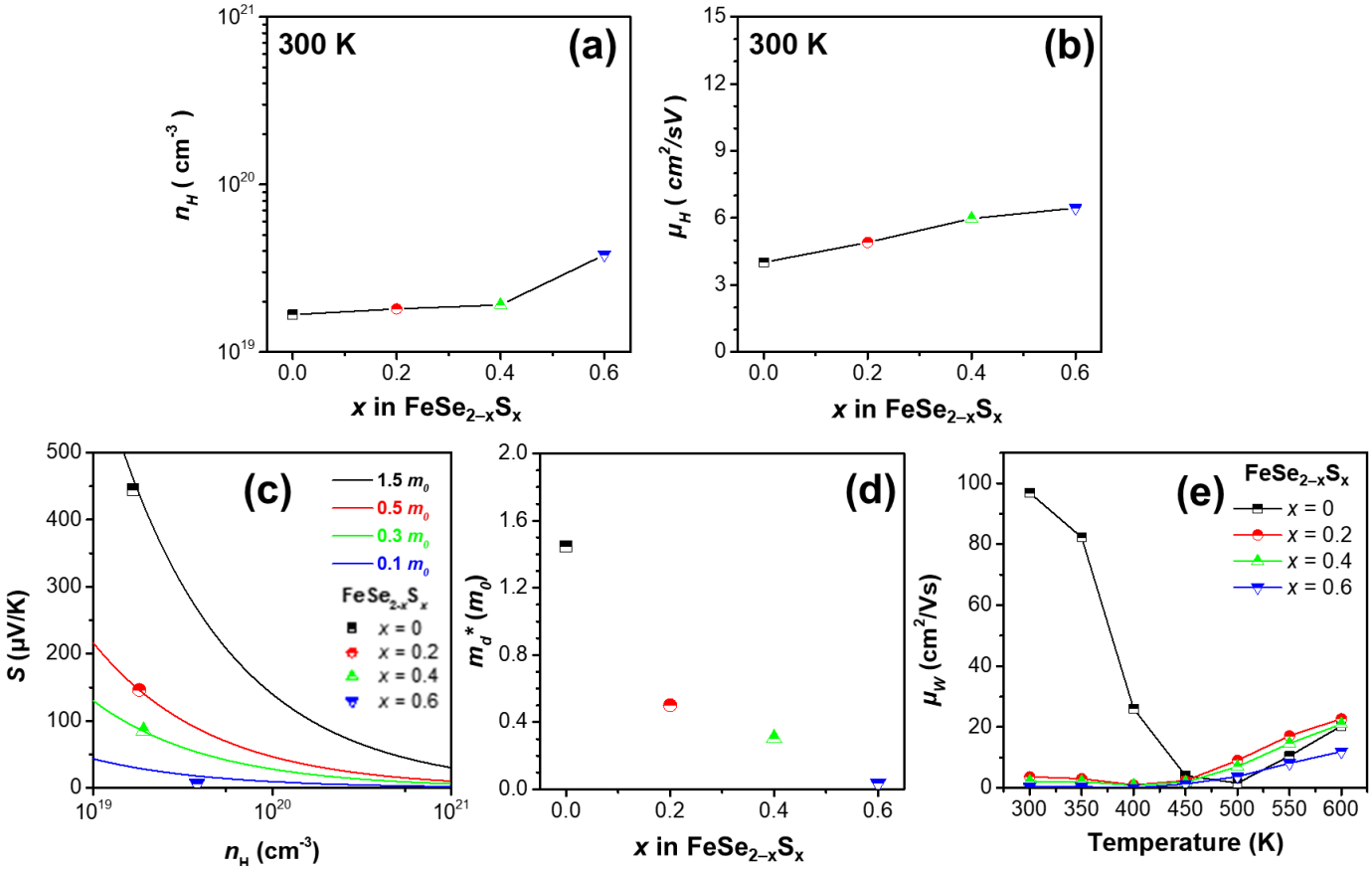


Figure 3. (**a**) n_H and (**b**) μ_H of the series of $FeSe_{2-x}S_x$ (x = 0, 0.2, 0.4, and 0.6) samples. (**c**) S as a function of n_H (Pisarenko plot) at 300 K. (**d**) m_d^* as a function of x in $FeSe_{2-x}S_x$ (x = 0, 0.2, 0.4, and 0.6). (**e**) μ_w as a function of temperature for the samples.

Figure 4c,d shows the calculated zT values of p- and n-type conduction, respectively. In Figure 4c, the maximum zT of the pristine sample was ~0.02, and the alloyed samples exhibited even lower zT values below 0.005. On the other hand, in Figure 4d of n-type conduction of high-temperature range, the samples with x = 0.2 and 0.4 exhibited zT values higher than that of the pristine sample, mainly owing to the decrease in κ_{tot}. Consequently, the $FeSe_{1.8}S_{0.2}$ (x = 0.2) sample exhibited a maximum zT value of 0.079, which was approximately 18% higher than that of the pristine $FeSe_2$ sample.

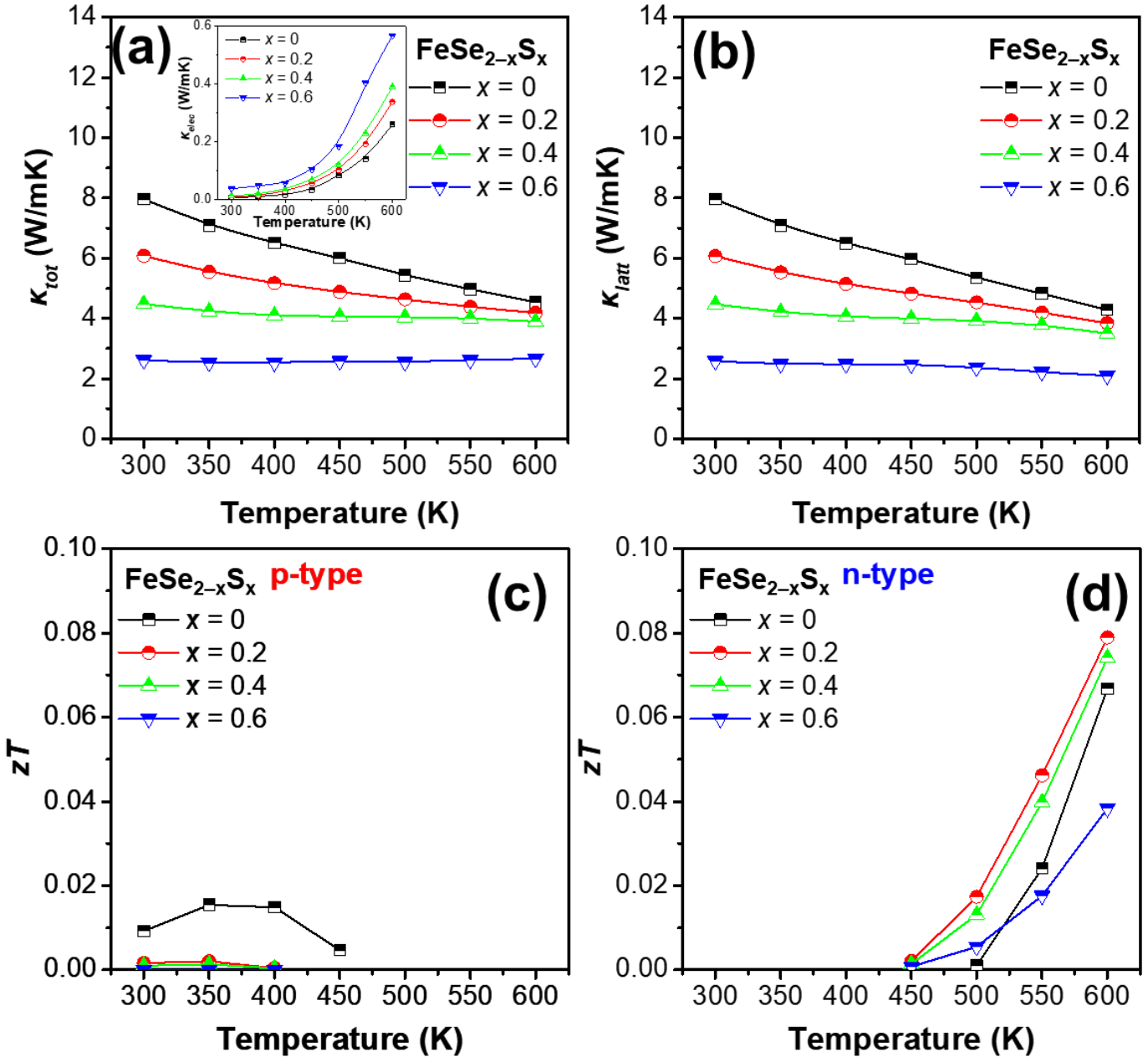


Figure 4. (**a**) κ_{tot} and (**b**) κ_{latt} as functions of temperature for the series of $FeSe_{2-x}S_x$ (x = 0, 0.2, 0.4, and 0.6) samples. The inset of (**a**) shows κ_{elec} as a function of temperature for the samples. zT as a function of temperature for the samples in (**c**) p- and (**d**) n-type regions.

4. Conclusions

A series of $FeSe_{2-x}S_x$ (x = 0, 0.2, 0.4, 0.6, and 0.8) polycrystalline samples were synthesized by a conventional solid-state reaction, and their thermoelectric transport properties were examined in an effort to search for the cost-effective thermoelectric materials. A single orthorhombic $FeSe_2$ phase was successfully synthesized for x = 0, 0.2, and 0.4; however, a secondary phase (Fe_7S_8 or FeS_2) was identified for x = 0.6 and 0.8. The lattice parameters decreased gradually with an increase in S content for $x < 0.8$, suggesting that S atoms were substituted at the Se sites in the $FeSe_2$ crystal structure. The electrical conductivity increased gradually with an increase in S content, whereas the magnitude of S decreased gradually with an increase in S content. As a result, the sample with x = 0.2 exhibited a maximum power factor of 0.55 mW/mK^2 at 600 K. The total thermal conductivity decreased

significantly with an increase in S content, and thus a maximum thermoelectric figure of merit value of 0.079 was obtained for the $FeSe_{1.8}S_{0.2}$ (x = 0.2) sample at 600 K, which was approximately 18% higher than that of the $FeSe_2$ (x = 0) sample.

Supplementary Materials: The following supporting information can be downloaded at: https://www.mdpi.com/article/10.3390/mi13122066/s1, Figure S1: EDS-SEM results for $FeSe_{2-x}S_x$ (x = 0, 0.2, 0.4, 0.6 and 0.8); Figure S2: (a) σ, (b) S, and (c) PF as a function of temperature for the $FeSe_2$ sample, measured after ~180 days from the initial measurement for cycling test; Figure S3: Estimated E_g for the series of $FeSe_{2-x}S_x$ (x = 0, 0.2, 0.4 and 0.6) samples using Goldsmid-Sharp empirical formular; Table S1: The relative peak intensities for (111), (012), (121), (011), (200) and (103) planes for $FeSe_{2-x}S_x$ (x = 0, 0.2, 0.4, and 0.6) in the X-ray diffraction data; Table S2: Atomic ratios measured by EDS-SEM for $FeSe_{2-x}S_x$ (x = 0, 0.2, 0.4, 0.6 and 0.8). References [16,28] are cited in the supplementary materials.

Author Contributions: Conceptualization, S.-i.K.; investigation, O.P. and S.W.L.; data curation, O.P. and S.W.L.; writing—original draft preparation, O.P., S.W.L., and S.J.P.; writing—review and editing, S.-i.K.; project administration, S.-i.K.; funding acquisition, S.-i.K. All authors have read and agreed to the published version of the manuscript.

Funding: This study was supported by the National Research Foundation of Korea (NRF-2019R1C1 C1005254, and NRF-2022R1F1A1063054).

Data Availability Statement: Data available upon reasonable request.

Conflicts of Interest: The authors declare no conflict of interest.

References

1. Flipse, J.; Bakker, F.L.; Slachter, A.; Dejene, F.K.; van Wees, B.J. Direct observation of the spin-dependent Peltier effect. *Nat. Nanotechnol.* **2012**, *7*, 166–168.
2. Tritt, T.M.; Subramanian, M.A. Thermoelectric Materials, Phenomena, and Applications: A Bird's Eye View. *MRS Bull.* **2006**, *31*, 188–198. [CrossRef]
3. Gaultois, M.W.; Sparks, T.D.; Borg, C.K.H.; Seshadri, R.; Bonificio, W.D.; Clarke, D.R. Data-Driven Review of Thermoelectric Materials: Performance and Resource Considerations BT—Chemistry of Materials. *Chem. Mater.* **2013**, *25*, 2911–2920. [CrossRef]
4. Zhao, K.; Guan, M.; Qiu, P.; Blichfeld, A.B.; Eikeland, E.; Zhu, C.; Ren, D.; Xu, F.; Iversen, B.B.; Shi, X.; et al. Thermoelectric Properties of $Cu_2Se_{1-x}Te_x$ Solid Solutions. *J. Mater. Chem. A* **2018**, *6*, 6977–6986. [CrossRef]
5. Skoug, E.J.; Cain, J.D.; Morelli, D.T. High thermoelectric figure of merit in the Cu_3SbSe_4-Cu_3SbS_4 solid solution. *Appl. Phys. Lett.* **2011**, *98*, 261911. [CrossRef]
6. Xing, T.; Zhu, C.; Song, Q.; Huang, H.; Xiao, J.; Ren, D.; Shi, M.; Qiu, P.; Shi, X.; Xu, F.; et al. Ultralow Lattice Thermal Conductivity and Superhigh Thermoelectric Figure-of-Merit in (Mg, Bi) Co-Doped GeTe. *Adv. Mater.* **2021**, *33*, 2008773. [CrossRef]
7. Asfandiyar, T.-R.W.; Li, Z.; Sun, F.-H.; Pan, Y.; Wu, C.-F.; Farooq, M.U.; Tang, H.; Li, F.; Li, B.; Li, J.-F. Thermoelectric SnS and SnS-SnSe solid solutions prepared by mechanical alloying and spark plasma sintering: Anisotropic thermoelectric properties. *Sci. Rep.* **2017**, *7*, 43262. [CrossRef]
8. Bang, J.; Kim, H.-S.; Kim, D.H.; Lee, S.W.; Park, O.; Kim, S.-I. Phase formation behavior and electronic transport properties of $HfSe_2$-$HfTe_2$ solid solution system. *J. Alloys Compd.* **2022**, *920*, 166028. [CrossRef]
9. Song, H.-Y.; Sun, J.-J.; Li, M. Enhancement of monolayer $HfSe_2$ thermoelectric performance by strain engineering: A DFT calculation. *Chem. Phys. Lett.* **2021**, *784*, 139109. [CrossRef]
10. Abdollah, H.M.; Mohammad, Y.; Mojtaba, Y.; Alireza, A. Investigation into thermoelectric properties of M (M = Hf, Zr) X_2 (X = S, Se, Te) nanotubes using first-principles calculation. *Solid State Commun.* **2021**, *336*, 114289. [CrossRef]
11. Kumar, S.; Schwingenschlögl, U. Thermoelectric Response of Bulk and Monolayer $MoSe_2$ and WSe_2. *Chem. Mater.* **2015**, *27*, 1278–1284. [CrossRef]
12. Luo, Y.; Zheng, Y.; Luo, Z.; Hao, S.; Du, C.; Liang, Q.; Li, Z.; Khor, K.A.; Hippalgaonkar, K.; Xu, J.; et al. *n*-Type $SnSe_2$ Oriented-Nanoplate-Based Pellets for High Thermoelectric Performance. *Adv. Energy Mater.* **2018**, *8*, 1702167. [CrossRef]
13. Kim, S.-I.; Bang, J.; An, J.; Hong, S.; Bang, G.; Shin, W.H.; Kim, T.; Lee, K. Effect of Br substitution on thermoelectric transport properties in layered $SnSe_2$. *J. Alloys Compd.* **2021**, *868*, 159161. [CrossRef]
14. Mavrokefalos, A.; Nguyen, N.T.; Pettes, M.T.; Johnson, D.C.; Shi, L. In-plane thermal conductivity of disordered layered WSe_2 and $(W)_x(WSe_2)_y$ superlattice films. *Appl. Phys. Lett.* **2007**, *91*, 171912. [CrossRef]
15. Guo, Z.; Zhao, R.; Yan, S.; Xiong, W.; Zhu, J.; Lu, K.; Wang, X. Atomic Layer Deposition of $FeSe_2$, $CoSe_2$, and $NiSe_2$. *Chem. Mater.* **2021**, *33*, 2478–2487. [CrossRef]
16. Li, G.; Zhang, B.; Rao, J.; Herranz Gonzalez, D.; Blake, G.R.; de Groot, R.A.; Palstra, T.T. Effect of vacancies on magnetism, electrical transport, and thermoelectric performance of marcasite $FeSe_{2-\delta}$ (δ = 0.05). *Chem. Mat.* **2015**, *27*, 8220. [CrossRef]

17. Gudelli, V.K.; Kanchana, V.; Vaitheeswaran, G.; Valsakumar, M.C.; Mahanti, S.D. Thermoelectric properties of marcasite and pyrite FeX_2 (X = Se, Te): A first principle study. *RSC Adv.* **2014**, *4*, 9424. [CrossRef]
18. Park, O.; Kim, T.; Lee, S.W.; Kim, H.-S.; Shin, W.H.; Rahman, J.U.; Kim, S.-I. Study of Phase Formation Behavior and Electronic Transport Properties in the $FeSe_2$-$FeTe_2$ System. *Korean J. Met. Mater.* **2022**, *60*, 315–320. [CrossRef]
19. Zuniga-Puelles, E.; Cardoso-Gil, R.; Bobnar, M.; Veremchuk, I.; Himcinschi, C.; Hennig, C.; Kortus, J.; Heide, G.; Gumeniuk, R. Structural stability and thermoelectric performance of high quality synthetic and natural pyrites (FeS_2). *Dalton Trans.* **2019**, *48*, 10703–10713. [CrossRef]
20. Harran, I.; Li, Y.; Wang, H.; Chen, Y.; Ni, Y. Iron Disulfide Compound: A Promising Thermoelectric Material. *Mater. Res. Express* **2017**, *4*, 105907. [CrossRef]
21. Gronvold, F.; Westrum, E.F., Jr. Heat capacities of iron disulfides Thermodynamics of marcasite from 5 to 700 K, pyrite from 300 to 780 K, and the transformation of marcasite to pyrite. *J. Chem. Thermodyn.* **1976**, *8*, 1039–1048. [CrossRef]
22. Patterson, A.L. The Scherrer Formula for X-Ray Particle Size Determination. *Phys. Rev.* **1939**, *56*, 978–982. [CrossRef]
23. Yoo, J.; Kim, J.-I.; Cho, H.-J.; Choo, S.-S.; Kim, S.-I.; Lee, K.; Shin, W.H.; Kim, H.-S.; Roh, J.W. Electronic and Thermal Properties of Si-doped InSe Layered Chalcogenides. *J. Korean Phys. Soc.* **2018**, *72*, 775–779. [CrossRef]
24. Ioffe, A.F. *Physics of Semiconductors*; Academic Press: New York, NY, USA, 1960.
25. Snyder, G.J.; Snyder, A.H.; Wood, M.; Gurunathan, R.; Snyder, B.H.; Niu, C. Weighted mobility. *Adv. Mater.* **2020**, *32*, 2001537. [CrossRef]
26. Kim, M.; Kim, S.-I.; Kim, S.W.; Kim, H.-S.; Lee, K.H. Weighted mobility ratio engineering for high-performance Bi-Te-based thermoelectric materials via suppression of minority carrier transport. *Adv. Mater.* **2021**, *33*, 2005931. [CrossRef]
27. Lorenz, L. Determination of the degree of heat in absolute measure. *Ann. Phys. Chem.* **1872**, *147*, 429–451. [CrossRef]
28. Goldsmid, H.J.; Sharp, J.W. Estimation of the thermal band gap of a semiconductor from seebeck measurements. *J. Electron. Mater.* **1999**, *28*, 869–872. [CrossRef]